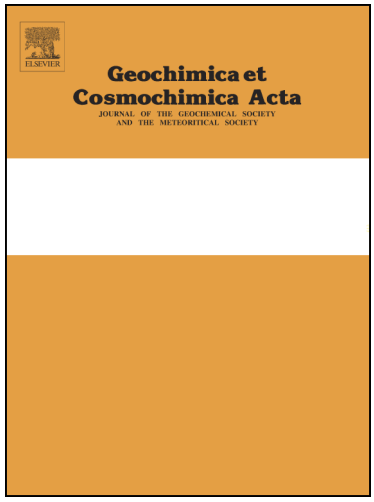

High temperature (> 350 °C) thermochronology and mechanisms of Pb loss in apatite

Ryan Cochrane, Richard A Spikings, David Chew, Jörn-Frederik Wotzlaw, Massimo Chiaradia, Shane Tyrrell, Urs Schaltegger, Roelant Van der Lelij

PII: S0016-7037(13)00667-4
DOI: http://dx.doi.org/10.1016/j.gca.2013.11.028
Reference: GCA 8561

To appear in: *Geochimica et Cosmochimica Acta*

Received Date: 16 April 2013
Accepted Date: 19 November 2013

Please cite this article as: Cochrane, R., Spikings, R.A., Chew, D., Wotzlaw, r-F., Chiaradia, M., Tyrrell, S., Schaltegger, U., Lelij, R.V.d., High temperature (> 350 °C) thermochronology and mechanisms of Pb loss in apatite, *Geochimica et Cosmochimica Acta* (2013), doi: http://dx.doi.org/10.1016/j.gca.2013.11.028

High temperature (> 350 °C) thermochronology and mechanisms of Pb loss in apatite

Ryan Cochrane[1]*, Richard A Spikings[1], David Chew[2], Jörn-Frederik Wotzlaw[1], Massimo Chiaradia[1], Shane Tyrrell[3], Urs Schaltegger[1], Roelant Van der Lelij[1]

Affiliations:

[1]Section of Earth and Environmental Sciences, University of Geneva, Switzerland (ryan.cochrane@unige.ch)

[2] Department of Geology, School of Natural Sciences, Trinity College Dublin, Ireland

[3] UCD School of Geological Sciences, University College Dublin, Ireland

Abstract

Natural processes driven by heat flow can be understood using quantitative reconstruction of the thermal history of accessory and common minerals that were formed or modified in these processes. Thermochronology assumes that isotopes are lost from minerals by thermally-activated volume diffusion, and forms the basis of many studies of the thermal evolution of the crust. However, some studies challenge this assumption and suggest that the mechanisms controlling isotope transport in minerals over geological time-scales are dominated by aqueous fluid flow within mineral pathways. Here, we test these contrasting hypotheses by inverse modelling apatite uranium-lead (U-Pb) dates to produce theoretical t-T solutions assuming Pb was lost by volume diffusion. These solutions are compared with independent geological constraints and intra-grain apatite U-Pb dates, which demonstrate that volume diffusion governed the displacement of Pb. This confirmation, combined with an inverse-modeling procedure that

permits reheating and cooling paths to be distinguished between ~375 - 570 °C, provides geologists with a unique tool for investigating the high-temperature thermal evolution of accessory minerals using the U-Pb method.

Key words: U-Pb thermochronology, volume diffusion, inverse-modeling.

1. Introduction

The thermal histories of accessory and some common minerals in the Earth, planets and meteorites can provide key information to investigate fundamental processes ranging from planetary accretion and the timing of impact events (Weiss et al., 2002), to plate tectonics, formation of mountains, and the evolution of sedimentary basins (Spikings et al., 2010). Thermochronological methods such as ^{238,235}U-^{206,207}Pb (accessory phases, e.g. apatite, titanite, rutile), ^{40}Ar/^{39}Ar (alkali feldspars), fission track and (U-Th-Sm)/He dating are tools that constrain the thermal histories of accessory and common minerals (e.g. Watson and Baxter, 2007). These methods rely on the fundamental assumption that the radiogenic isotopes produced (e.g. ^{206,207}Pb, ^{40}Ar and ^{4}He) are redistributed within minerals and ultimately lost to an infinite reservoir by thermally activated, volume diffusion (Blackburn et al., 2011; Cassata et al., 2009; Chamberlain and Bowring, 2001; Harrison et al., 2009; Lovera et al., 1997; Schoene et al., 2007; Wartho et al., 1999). Previous studies have supported this assumption over laboratory time-scales (i.e. hours to months), under controlled conditions (Cherniak et al., 1991; Cherniak et al., 2004). However, several authors have suggested that the physical mechanisms that control isotope transport through crystal lattices over geological time-scales in nature are dominated by aqueous fluid flow along distinct pathways (Fig. 1) during metamorphic retrogression, and that

thermally activated diffusion is of secondary importance (Lee, 1995; Villa, 1998). Experimental verification of the role played by volume diffusion in mechanisms of daughter isotope loss over geological time-scales is therefore paramount in validating the accuracy of thermochronological studies.

We present U-Pb isotopic data from natural apatites of variable grain sizes that are used to test the hypothesis that thermally activated volume diffusion over geological timescales controlled the loss of Pb. Confirmation of the hypothesis will establish the apatite U-Pb system as a reliable thermochronometer, suggesting that fluid assisted Pb loss plays an insignificant role. A majority of thermochronological studies have focused on isotopic systems that are sensitive to temperatures of ~350-40 °C (Gallagher et al., 1998; Quidelleur et al., 1997; Spikings et al., 2002), whereas significantly fewer studies (e.g. Blackburn et al., 2012; Schoene and Bowring, 2007) have utilised methods that are sensitive to higher temperatures. The U-Pb system in most accessory phases (e.g. apatite and titanite) is sensitive to temperatures >350 °C (Blackburn et al., 2011), and therefore can provide Earth scientists with a unique tool to understand i) how lower crustal rocks are exhumed, ii) the tectonic stability of the lower crust and cratons, and iii) the tectonic history of active margins over long time periods (e.g. 500 Ma), during which they may have experienced numerous terrane collision events and a substantial amount (> 15 km) of exhumation. The high temperature sensitivity of the U-Pb method also renders is suitable to investigate extra-terrestrial processes such as planetary accretion rates, and asteroid impact and ejection events. Alternatively, negation of the hypothesis would suggest that age variations may reflect interaction with aqueous fluids (e.g. short-circuit diffusion; Fig. 1) during retrogression or growth during prograde metamorphism (Nutman et al., 2007). This conclusion would imply that

extreme caution should be used when attempting to extract thermal history information from apatite U-Pb dates.

A secondary aim of this manuscript is to describe the advantage gained by combining independent U-Pb data sets obtained using Isotope Dilution-Thermal Ionization Mass Spectrometry (ID-TIMS) and Multi Collector-Laser Ablation-Inductively Coupled Plasma Mass Spectrometry (MC-LA-ICP-MS) when extracting thermal history information from U-Pb dates. Both data sets can be used to reconstruct statistically likely thermal histories, and the histories obtained from each method should be indistinguishable. Previous U-Pb thermochronological studies have shown that the U-Pb method can be used to differentiate between time(t)-Temperature(T) paths that are characterized by re-heating and gradual cooling when U-Pb concordia space is used (Blackburn et al., 2011). However, this approach is impractical for younger (e.g. Phanerozoic) t-T paths, where the large age uncertainties often result in concordant dates despite the fact that they have demonstrably experienced lead loss. This limitation is particularly acute for apatite, which has low radiogenic to initial common Pb ratios (Pb^*/Pb_c), typically resulting in relatively large age uncertainties. However, re-heating and gradual cooling or isothermal holding results in different core-rim intra-grain patterns of U-Pb dates, and this study measures apatite in-situ dates in an attempt to resolve between re-heating and slow-cooling paths.

2. The case study

2.1 Geological Framework

Palaeozoic – Early Cretaceous metamorphic rocks of the Eastern Cordillera of Ecuador formed the Early Cretaceous active margin of northwestern South America (Fig. 2). The oldest rocks

exposed are undifferentiated Palaeozoic metasedimentary rocks (Chiguinda Formation), which were melted to varying degrees and intruded by juvenile mafic melts during continental rifting within western Pangaea in the Triassic (Litherland et al., 1994; Cochrane, 2013). The crustal anatectites include massive granitic bodies (Tres Lagunas Granite) and extensive migmatites (Sabanilla Migmatites). A passive margin had developed by ~216 Ma, which became active at ~190 Ma, in Ecuador (Litherland et al., 1994). The Hf and Nd isotopic composition of volcanic rocks, combined with increasingly depleted geochemical compositions indicates that trenchward migration of continental arc magmatism during 145 – 115 Ma occurred during extension of the margin (Cochrane, 2013). The Caribbean Plateau and its overlying island arc collided with northwestern South America at ~75 Ma (Vallejo et al., 2009; Spikings et al., 2010; Villagomez and Spikings, 2013), resulting in rapid rock uplift and exhumation rates along the entire margin, forming the highlands of the Eastern Cordillera, and the Amazon Foreland Basin to the east. The Late Cretaceous - Miocene thermal and exhumation history of the Eastern Cordillera has been previously constrained using the $^{40}Ar/^{39}Ar$, fission track and (U-Th)/He methods (Spikings et al., 2000, 2001, 2010).

2.2 Experimental approach to testing the hypothesis

ID-TIMS U-Pb dates have been obtained from apatite extracted from a leucosome of a Triassic migmatite that crops out in the southern Eastern Cordillera of Ecuador (Fig. 2). The sampled region represents a superb natural laboratory to test the aforementioned hypothesis because its tectonic and low temperature (<350°C) thermal history is well-established (Spikings et al., 2010), and the margin has resided within a presumably fluid-rich, arc-environment since the Early Jurassic (Litherland et al., 1994). Thus, the competing effects of volume diffusion and

fluid-assisted Pb loss can be tested. Those single and multi-grain ($n \leq 4$) apatite U-Pb dates have been combined with experimentally determined diffusion parameters for Pb in apatite (Cherniak et al., 1991) to derive t-T solutions (using HeFTy version 1.7.0; Ketcham, 2005) for the migmatite by inverse-modeling of $^{206}Pb/^{238}U$ dates, assuming volume diffusion, using a brute-force Markov Chain Monte Carlo approach. The large quantity of iterations (> 1 million) that are tested during inverse modeling provides an opportunity to test whether or not Mesozoic apatite U-Pb dates can be used to differentiate between slow cooling and reheating at high (~375 – 570 °C) temperatures. The accuracy of the t-T solutions is tested by comparing the t-T solutions against independent geological constraints, and comparing predicted U-Pb date-profiles along transects from the cores to the rims of individual crystals with measured in-situ U-Pb dates of different apatites separated from the same leucosome. The in-situ dates have been obtained using LA-MC-ICP-MS.

3. Analytical methods

3.1 LA-ICP-MS zircon geochronology

U-Pb isotopic data was obtained from zircons extracted from leucosome RC42 using a Laser Ablation Inductively Coupled Mass Spectrometer (LA-ICP-MS; Fig. 2; Supplementary Table 1) housed at the University of Lausanne, Switzerland. The sample was crushed using a jaw crusher and zircons were concentrated using gravimetric and magnetic techniques. Inclusion free zircons were handpicked under a binocular microscope, mounted into epoxy blocks and polished to expose their grain interiors. Cathodoluminescence images of all zircons were obtained using a CamScan MV2300 scanning electron microscope and suitable zircons were ablated using a NewWave UP-193 ArF excimer ablation system. Analytical details are provided in the Appendix.

3.2 U-Pb dating of apatite using ID-TIMS

Inclusion- and crack-free euhedral apatite crystals with a large range in grain size were selected for ID-TIMS U-Pb geochronology. Selected apatite crystals were photographed and their grain sizes were measured in two orientations (parallel and perpendicular to the c-axis). Single or small multi-grain fractions (Table 1) were rinsed and washed with ultra-sound in ultrapure H_2O and acetone prior to loading in 3 ml Savillex beakers. Fractions were spiked with an appropriate amount of the Earthtime ^{205}Pb-^{233}U-^{235}U tracer solution (www.earth-time.org) and subsequently dissolved in 6M HCl for ~72 hours at 120°C on a hotplate. After dissolution, samples were dried down and re-dissolved in ~1M HBr. U and Pb were separated using a modified HBr-based (Krogh, 1973) single-column anion exchange chemistry. U and Pb fractions were loaded separately on outgassed zone-refined single Re filaments with a silica-gel/phosphoric acid emitter solution (Gerstenberger and Haase, 1997).

U and Pb isotopic compositions were measured on a Thermo Triton thermal ionization mass spectrometer (TIMS) at the University of Geneva Radiogenic Isotope Laboratory. Pb was measured using a dynamic peak jumping routine on a MasCom secondary electron multiplier (SEM). Mass fractionation on the electron multiplier was determined to be 0.13 ± 0.03 %/amu based on daily analyses of the NBS-981 common Pb standard. U was measured as U-oxide in static mode on Faraday cups equipped with 10^{12} Ω resistors, or using a dynamic peak jumping routine on the SEM. Measured isotopic ratios were corrected for interferences of $^{233}U^{18}O^{16}O$ on $^{235}U^{16}O_2$ using an $^{18}O/^{16}O$ of 0.00205, measured on large U500 loads, and mass fractionation was controlled using a double spike with a $^{233}U/^{235}U$ ratio of 0.99506. 0.9 ± 0.5 pg of the total common Pb was assigned to laboratory blank and the remaining common Pb was corrected using the

measured isotopic composition of co-genetic K-feldspars (see appendix). U-Pb ratios and dates were calculated relative to a $^{235}U/^{205}Pb$ ratio of 100.23 ± 0.023% (1σ) for the tracer and raw data were reduced using Tripoli and U-Pb_Redux software (Bowring et al., 2011; McLean et al., 2011). All uncertainties are reported at the 95% confidence level and exclude systematic uncertainties associated with tracer calibration and decay constants, unless otherwise indicated. The concordia plot is shown in Fig. 3.

Apatite crystals typically incorporate low quantities of uranium and significant amounts of lead during crystallization, resulting in low Pb*/Pbc in Phanerozoic samples (0.1 – 0.3 in this study). Therefore, an accurate knowledge of the initial Pb isotopic composition is required to obtain useful U-Pb dates.

3.3 U-Pb dating of apatite using LA-MC-ICPMS

U-Pb dates were also determined by LA-MC-ICPMS at the National Centre for Isotope Geochemistry at UCD, Dublin, Ireland using recently outlined procedures (Chew et al., in press). Analyses were carried out using a NEPTUNE MC-ICPMS system coupled to a New Wave Research 193nm excimer laser ablation system. A spot size of 15 µm was selected and a laser energy of 5.6 mJ with a repetition rate of 5Hz was used. Ion counters were used to measure ^{202}Hg, $^{204}Pb+Hg$, ^{206}Pb, ^{207}Pb and ^{238}U. Analyses included a 15 second gas blank, followed by a spot analysis with a dwell time of 60 seconds, the first 5 seconds of which was disregarded to avoid any elevated common Pb from surface contamination. Data were reduced and errors propagated using the freeware IOLITE data-reduction package (Paton et al., 2010) combined with the VizualAge data reduction scheme (Petrus and Kamber, 2012). This approach involves processing an entire analytical session of data, which is efficient and greatly improves the

consistency and reliability of data reduction. Laser-induced elemental (i.e. U-Pb) fractionation was corrected for by characterizing the time-resolved fractionation response of individual standard analyses, and then fitting an appropriate session-wide "model" U-Th-Pb fractionation curve to the time-resolved standard data. This fractionation model is then applied to the unknowns. Two apatite standards were used to monitor laser-induced elemental fractionation and instrument mass bias. These are Emerald Lake apatite (92.5 ± 3.3 Ma; Chew et al., 2011) and Durango apatite (31.44 ± 0.18 Ma; McDowell et al., 2005). Common Pb correction was undertaken using a ^{207}Pb-based correction (Williams, 1998). Analytical data are listed in Table 2.

3.4 ^{40}Ar/^{39}Ar analyses

Fresh muscovite was separated using a Wilfley table and a Frantz magnetic separator and cleaned in deionized water in an ultrasonic bath for 5 minutes before 3 milligrams of the cleanest, unaltered and inclusion free muscovite was picked under a binocular microscope. Muscovite crystals were irradiated for 30 hours at the TRIGA reactor (CLICIT facility) at Oregon State University, and Fish Canyon Sanidine (28.02±0.28 Ma; Renne et al., 1998) was used as the flux monitor. 1 mg of muscovite was analysed (Supplementary Table 2) by incremental step heating using a 55W CO_2-IR laser coupled to a stainless steel gas extraction line and a multi-collector mass spectrometer (Argus; Thermo Scientific) housed at the University of Geneva. Analytical details are provided in the appendix.

4. Results

4.1 U-Pb zircon analysis of leucosome RC42

Thirty five zircons analysed by LA-ICP-MS yielded concordant $^{206}Pb/^{238}U$ ages ranging between 1883 – 243 Ma (Supplementary Table 1). The youngest cluster of five concordant analyses yielded a weighted mean age of 247±4.3 Ma (MSWD 3.0; Figure 2c), which is interpreted to record the timing of anatexis, forming the leucosome from which the zircons and apatites were extracted. The older zircons are considered to be xenocrystic contamination from adjacent restite and melanosome.

4.2 U-Pb apatite data obtained using TIMS

The selected migmatite from the southern Ecuadorean Andes formed by Triassic anatexis of Permian sedimentary rocks at 247.0 ± 4.3 Ma (zircon U-Pb, LA-ICP-MS; Fig. 2). The crustal melting event occurred during Triassic continental extension and basaltic underplating, which lead to rifting (Litherland et al., 1994). We have selected inclusion-free, euhedral, stubby and hexagonal apatite crystals from a single leucosome (RC42). The apatites were divided into 14 aliquots according to their grain radii (~175-45 µm, effective diffusion radius) to test for length-scale dependent volume diffusion (Table 1). The measured apatite $^{206}Pb/^{238}U$ dates or either single or multiple grains were calculated using co-genetic K-feldspar Pb_c, and uncertainties ($^{206}Pb/^{204}Pb_i$, $^{207}Pb/^{204}Pb_i$ and $^{208}Pb/^{204}Pb_i$) on these measurements were propagated at 1.0, 0.5 and 1.5 %, respectively (Fig. 3; Table 1). We use these conservative uncertainty estimates to account for the inter- and intra-grain variability that is commonly observed in alkali feldspars (Table 1; Chamberlain and Bowring, 2001; Housh and Bowring, 1991).

Concordant $^{206}Pb/^{238}U$ dates range between 81.52 ± 2.61 and 137.46 ± 2.62 Ma (Fig. 3a), and show a positive correlation with grain radius (Figure 3b) for 11 of the size aliquots. Those 11 aliquots yield Th/U ratios of <0.18 (Figure 3c), which are consistent with magmatic apatites that

crystallized in the presence of monazite, which preferentially sequesters Th and other REE (Chu et al., 2009). Monazite is typically stable in peraluminous S-type granites and crustal anatectites (Chu et al., 2009). The tracer, fractionation and blank corrected $^{208}Pb/^{204}Pb$ ratios of most of the low Th/U apatites are indistinguishable from the $^{208}Pb/^{204}Pb$ ratios of the initial common Pb measured on co-genetic feldspar, assuming an uncertainty of 1.5% on the latter ratio. Consequently, the calculated Th/U ratios of these apatites are extremely sensitive to the common-Pb correction, resulting in a relative uncertainty higher than 100%. Considering these large uncertainties, all of the Th/U ratios of the low Th/U apatites are equivalent, and the apparent correlation between Th/U and U-Pb date (Fig. 3c) is an artifact of the common Pb correction. Three size aliquots yield anomalously high Th/U ratios (0.35 – 1.9), which may reflect a decreased modal presence of monazite within the environment within which they crystallised (e.g. I-type or Ca enriched granitic magmas; Chu et al., 2009). These relatively high Th/U apatites diverge from the grain size vs. date correlation (Figure 3b) and yield relatively young $^{206}Pb/^{238}U$ dates. Leucosome RC42 is a crustal anatectite with strongly peraluminous compositions (Cochrane, 2013), suggesting that the high Th/U apatites either host xenocrystic cores or are entirely xenocrystic.

4.3 U-Pb apatite data obtained using MC-LA-ICP-MS

Intra-grain U-Pb dates have been obtained from apatites extracted from the same leucosome, and which also have different grain radii, using LA-MC-ICP-MS. To best remove polishing bias effects and to reveal the entire diffusion length from core-rim (hexagonal geometry), apatites were mounted with their c-axes oriented parallel to the incident laser beam within small epoxy mounts, and polished to reveal their grain interiors (Fig. 4).

The apatites are homogeneous in electron backscatter images and were ablated using a 15 µm diameter laser beam along a series of rim-core-rim transects. Large crystals (~100 - 125 µm; Fig. 4a-c) show well-defined yet highly variable (~190-70 Ma), bell-shaped, core-rim age-profiles. The topology of the date-profiles from core-rim appears to relate partly to the uranium concentration, with zoned apatite exhibiting concave topologies and unzoned apatites yielding convex topologies. Smaller apatites (~45 – 55 µm, Fig. 4d-e) exhibit significantly less to no discernible variation in $^{206}Pb/^{238}U$ dates and cluster at ~70 Ma.

Diffusion theory suggests that when an age gradient exists within a sphere or infinite cylinder, the oldest ages will be located in the center of the grain or along the c-axis, assuming that the crystal is a single diffusion domain. However, some rim-core-rim date profiles are offset relative to the center of the section, and we attribute these to tilting of the grains during mounting (Fig. 4f). Unfortunately, even when the date profiles are not offset relative to the center of the section, and in the absence of precision mounting and crystallographic characterization, we cannot be certain that the c-axis has been ablated. We have not attempted to quantify the relationship between the distance of the spatial offset relative to the grain center, and variation in the statistically best-fitting t-T path. Rather, given the near symmetrical geometry of the crystal sections (Fig. 4), combined with careful mounting, we have assumed that the oldest ages and their uncertainties are a sufficient approximation of the location of the grain center, and inaccuracies in the preferred t-T paths have not been introduced.

4.4 $^{40}Ar/^{39}Ar$ analysis of muscovite extracted from leucosome RC42

Laser (CO_2) step-heating of pure, unaltered muscovite from leucosome RC42 yielded an undisturbed age spectrum (Table S2), with a plateau age of 71.46±0.33 Ma (Fig. 5), and an overlapping inverse isochron age of 71.41±0.40 Ma.

5. Interpretation

5.1 Relationship between apatite grain size and U-Pb dates

Eleven different size aliquots yield concordant $^{206}Pb/^{238}U$ dates that show a positive correlation with grain radius, which is consistent with thermally activated diffusive Pb loss (Fig. 3b). These apatites yield low Th/U ratios of <0.18, and crystallised within the leucosome. However, three size aliquots of apatite with higher Th/U ratios (0.35 – 1.9), which were also extracted from the leucosome but are interpreted to be at least partly xenocrystic, and yield $^{206}Pb/^{238}U$ dates that are young relative to their grain sizes and the prevailing trend.

Higher concentrations of parent isotopes (i.e. Th plus U) in the rims of apatite relative to the cores would yield younger ages than unzoned grains because the average diffusion length of the Pb ions would be shorter, yielding a lower bulk closure temperature (e.g. Farley et al., 2011). Therefore, the relatively younger $^{206}Pb/^{238}U$ dates yielded by the high Th/U apatites may be explained by U enriched rims, accelerated Pb loss due to metamictisation from alpha damage and ^{238}U-fission damage, or differences in intrinisic Pb diffusion characteristics within apatites due to differences in Th, REE and perhaps halogen concentrations. Unfortunately, we lack in-situ Th measurements and therefore we are unable to quantitatively determine core-rim variations in Th/U. All of the apatite grains dated using TIMS yielded similar $^{206}Pb/^{204}Pb$ ratios (~25 – 39; Table 1) suggesting similar bulk grain concentrations of U, whereas the Th/U ratios vary from ~0.03 to ~1.9. Therefore, the only differences (with respect to alpha damage) between the high

and low Th/U grains should be the radiation damage caused by ^{232}Th alpha decay. Considering ^{232}Th alpha decay has a half-life of ~14 Ga compared to ~4.47 Ga for ^{238}U (Steiger and Jager, 1977), the effect of alpha decay damage should be relatively minor. It is also likely that fission track and alpha damage would be annealed (e.g. Cherniak et al., 1991) within the temperature range of the PbPRZ, and hence variations in crystallinity are not invoked as the prime cause of the variation of dates relative to Th/U. Elevated Th concentrations in apatite may be coupled with elevated REE and halogen content (Chu et al., 2009) and this situation may arise when apatites crystallize from relatively calcium enriched magmas where monazite is unstable. Higher concentrations of halogens and REE, which significantly alter the annealing kinetics of fission tracks in apatite (Carlson et al., 1999), may also affect the diffusion properties of Pb. Regardless of the cause, those apatites with anomalously high Th/U ratios have been discarded from further consideration in this study.

5.2 The generation of theoretical t-T paths using the apatite U-Pb data

Thermal history solutions have been generated by inverse-modeling of ^{206}Pb/^{238}U (TIMS) dates obtained from six size aliquots, which best represent the date and grain size variation within the sample (Fig. 6). No more than 7 aliquots can be modeled simultaneously using HeFTy, and the selected 6 aliquots best represent the range of dates and grain sizes in the sample, and lie on the grain size v U-Pb date trend that is consistent with thermally activated diffusion. Due to the relatively large uncertainties associated with the measurements, all six aliquots yield 'concordant' dates and Pb loss cannot be identified within concordia space. This inverse modeling approach assumes that all Pb re-distribution and ultimately loss from the apatite crystals occurred by volume diffusion, and utilizes established Pb-in-apatite diffusion and spherical geometry (Cherniak et al.,

1991) characteristics. A spherical geometry has been utilized because it is the only geometry permitted by the software "HeFTy". However, there is no evidence that Pb diffusion in apatite is strongly anisotropic (e.g. Cherniak, 2010), and therefore a spherical geometry is valid. Furthermore, the temperature range of the bulk PbPRZ for an infinite cylinder geometry is only ~5°C higher than that for a spherical geometry (supplementary Figure S1), and it is unlikely that the topology of the t-T models generated assuming a sphere or infinite cylinder, or the timing and temperature of each inflexion point would be significantly different. The temperature range of the Pb Partial Retention Zone (PbPRZ) for these apatites is calculated assuming volume diffusion, and is defined as the range of closure temperatures (Dodson, 1986) calculated from the core of the largest grain (112 um), to the rim of the smallest grain (47 um), yielding values of 569°C and 375°C (assuming cooling rates of 20°C/Ma), respectively. Supplementary Figure S2 shows the relationship between the temperature bounds of the PbPRZ and grain size. $^{206}Pb/^{238}U$ dates were inverted using the software "HeFTy V1.7.0" (Ketcham, 2005), which uses a controlled random search procedure. Input parameters are experimentally determined parameters for the absolute diffusivity (Do) and activation energy (ΔEact) of Pb diffusion in apatite (Cherniak et al., 1991), grain radii (diffusion length) for six size aliquots, U concentration in each size aliquot from core to rim, and $^{206}Pb/^{238}U$ date for each aliquot.

The low radiogenic to common Pb (Pb*/Pbc = 0.1-0.3) of the apatites indicates that the calculated dates are strongly controlled by estimates of the common Pb composition. Consequently, our chosen uncertainties for the common Pb measurements of co-genetic alkali feldspar are large, and the calculated U-Pb dates overlap with dates obtained using common lead determined from the model of Stacey and Kramers (1975; for ages of 100 to 300 Ma). Therefore,

we are confident that the computed t-T paths are not unnecessarily biased by our choice of common lead correction.

Calculation of a theoretical $^{206}Pb/^{238}U$ date for any particular t-T path is performed by the net summation of the in-growth and diffusive loss of ^{206}Pb over the entire time span of the simulation. The controlled random search procedure generates random t-T paths whose form is biased according to input constraints, and compares the theoretical $^{206}Pb/^{238}U$ dates against the measured dates for each size aliquot. A Goodness-Of-Fit (GOF) is assigned to each iteration, which is a statistical function of the deviation of the modeled from the measured date (Ketcham, 2005). Solutions are generated with the assumption that the uncertainty of the measured date ($^{206}Pb/^{238}U$) is distributed normally in relation to the measured value. An acceptable-fit (GOF > 0.05) implies that 5 % of the possible samples within the data distribution are offset in their model age with respect to the measured age.

The iterations were given considerable freedom in t-T space, and were only constrained by the zircon crystallization age, and low temperature (<350°C) thermochronological constraints (boxes 2, 3 and 4 in Fig. 6b). The best-fit solutions yield a diffusion length vs. model date trend that overlaps with the diffusion length vs. measured date trend (Fig. 6a), are consistent with a weighted mean $^{40}Ar/^{39}Ar$ date (muscovite) of 71.46 ± 0.33 Ma (Fig. 5) obtained from the same leucosome, and are compatible with a large quantity of published zircon and apatite fission track and (U-Th)/He data from the same Triassic belt (Spikings et al., 2010). Importantly, the topology of the best-fit t-T solutions remains unchanged when the model is not constrained by the low temperature thermochronology data.

5.3 Testing the accuracy of the t-T solutions: comparison with geological constraints

The best-fit t-T solutions suggest that subsequent to anatexis at ~247 Ma, the migmatite rapidly cooled to temperatures colder than the bulk PbPRZ and resided there until ~140 Ma. The sample was steadily heated to temperatures within the bulk PbPRZ until 80-75 Ma, at which time it started to rapidly cool to temperatures colder than the bulk PbPRZ. The U-Pb apatite data no longer constrain the timing of inflexion points, or cooling and heating rates once the sample cooled below the temperature bounds of the PbPRZ. The timing of the inflexion points is consistent (within 5 Ma) with a detailed tectonic model (Cochrane, 2013; Spikings et al., 2001; Spikings et al., 2010; Vallejo et al., 2009) that was developed using independent sedimentological, geochronological and low temperature (<350°C) thermochronological data. That model concluded that Permian sedimentary rocks underwent anatexis in the Triassic and resided in the foreland region of a Jurassic arc. These rocks were later buried beneath an Early Cretaceous intra-arc basin that started opening at 145-140 Ma, and were subsequently exhumed during collision of the Caribbean Plateau at 75-73 Ma. Heating during ~140-80 Ma was a consequence of i) sedimentary burial, and ii) increased heat flow during extension.

5.4 Testing the accuracy of the t-T solutions: Comparing predicted and observed intra-grain apatite U-Pb dates

Theoretical core-to-rim U-Pb date profiles have been generated (Fig. 7) from the best-fit t-T solutions presented in Fig. 6b, and are compared with measured intra-grain $^{206}Pb/^{238}U$ LA-MC-ICP-MS dates (Fig. 4) to test the accuracy of the assumption that Pb has been lost by thermally activated, volume diffusion. Intra-grain diffusion profiles can also be mathematically determined directly from the relationship between grain size and U-Pb date (obtained using TIMS), although we wish to test the accuracy of the inversion modeling process and the t-T solutions. Theoretical

date vs. distance from core profiles have been determined for one of the best-fit t-T solutions, whose dominant characteristic is a period of reheating to a temperature within the bulk PbPRZ of the apatites, isothermal holding within the PbPRZ for longer than 100 My, and slow, linear cooling through the PbPRZ. Theoretical core-rim date profiles were made assuming both a homogeneous uranium concentration, and a heterogeneous concentration (determined from the in-situ U isotopic measurements; Table 2) where the cores of the grains are enriched relative to the rims. Core-to-rim variations in U concentration yield different theoretical Pb concentration profiles (normalized to the concentration of Pb at the grain core) because of a combination of i) apatites with higher concentrations of uranium in the core yield higher concentrations of Pb, and thus a core-rim Pb concentration gradient prior to diffusive Pb-loss during reheating into the bulk PbPRZ, and ii) during reheating, the percentage Pb loss at any location within the grain volume is the same for both the unzoned and zoned apatites, because they both followed the same t-T path.

Considering the best-fit t-T solution for the Triassic leucosome (Fig. 7a), thermally activated diffusive loss of Pb since anatexis at ~247 Ma predicts that almost all Pb was lost from the small grains during (~145 – 80 My) reheating to ~525°C. During this reheating period, the larger grains only experienced partial Pb loss, which created a significant core-rim Pb concentration gradient. Subsequent rapid cooling (80-75 Ma) of the sample to <375°C resulted in almost 100% retention of Pb in both cores and rims of the smaller grains. Apatites with uranium enriched cores (e.g. grains a and b; Fig. 4) yield intra-grain $^{206}Pb/^{238}U$ dates that follow a concave topology from core to rim, which with the exception of the rims, overlaps with the predicted date profiles obtained by forward modeling of a grain with the same core-rim distribution of uranium (Fig. 7a) along the best-fit thermal history path. A comparison of the

measured intra-grain $^{206}Pb/^{238}U$ dates with the theoretical date profiles obtained from isothermal holding (Figs 7b and 7c) and slow cooling (Fig. 7d) scenarios reveal poor fits. The discrepancy of the measured in-situ and predicted U-Pb dates of grains a and b at their rims may relate to the resolution of the core-rim U concentration measurements. The predicted age profiles assume a gradual variation of U along a particular trend from core to rim, whereas the in-situ dates relate to the measurement of U in 8 locations from core-rim, which do not spatially overlap (Fig. 4). Therefore, it is possible that the U concentrations at the outer rims may be different from what was assumed during the generation of the predicted dates at the rims. For example, a lower concentration of uranium at the rims would result in an older U-Pb date at the rim due to the introduction of parentless Pb from the interior.

The close fit of the core-rim date ($^{206}Pb/^{238}U$) profiles predicted by the best-fit t-T model, and the measured intra-grain dates strongly supports the hypothesis that Pb has been lost from the apatite crystals by thermally activated, volume diffusion. Inverting $^{206}Pb/^{238}U$ TIMS bulk grain dates to generate t-T models can resolve between reheating to within the PbPRZ (~375 - 570°C), and slow cooling through the PbPRZ for young (e.g. Mesozoic) samples (see below).

6. Discussion

6.1 Thermochronometry, recrystallization or interaction with aqueous fluids

Recrystallisation of apatite at times during 140 – 80 Ma (range of the U-Pb dates obtained by TIMS) would invalidate the thermochronological interpretations presented here. However, several lines of evidence demonstrate that Pb was lost from the apatite by thermally activated, volume diffusion over geological timescales. Pb loss mechanisms (Fig. 1; Lee, 1995; Villa, 1998) advocating an interaction with aqueous fluids (e.g. short-circuit pathways) are not required

to explain the single crystal and intra-grain U-Pb apatite dates. It is extremely unlikely that the trends in intra-grain U-Pb dates are a consequence of recrystallisation or sporadic growth (over ~120 Ma) of metamorphic or authigenic apatite because i) the small grains show no discernible variation in age from core to rim, ii) it would be fortuitous if recrystallisation of the large grains generated an intra-grain U-Pb core-rim age profile that matched predictions made by volume diffusion, and iii) back-scatter electron and cathodoluminsescence imaging of the apatites reveal no intra-grain discontinuities which could be interpreted as discrete growth domains or pathways for fluid infiltration. Previous studies have demonstrated the existence of thermally activated, volume diffusion of ions in mineral lattices over laboratory time-scales (Cherniak et al., 1991; Cherniak et al., 2004). Furthermore, Schoene et al. (2007) and Blackburn et al. (2011) have demonstrated that Pb is mobilized in apatite and other minerals by volume diffusion over geological timescales, although those studies solely relied on the relationship between diffusion length (grain size) and U-Pb date. This study is the first to combine bulk (TIMS) and intra-grain (LA-MC-ICP-MS) dates to demonstrate unambiguously that thermally activated, volume diffusion is responsible for the displacement and removal of Pb over geological time-scales. This confirms that apatite U-Pb dates can be used to perform quantitative thermochronometry.

6.2 Resolving between reheating and slow cooling

A great majority of best-fit t-T solutions in this study reveal a period of reheating (Fig. 6b), while <0.1% of the solutions permit isothermal holding and no plausible-fits were found for paths that describe gradual cooling through the temperature range of the PbPRZ. Regarding plate tectonic applications, these three different t-T forms imply distinctly different histories, and the ability to resolve them is pivotal. To understand further why inversion of the measured $^{206}Pb/^{238}U$ TIMS

dates favors re-heating, we have generated theoretical single-grain U-Pb dates for apatites with the same grain radii as those used throughout this study, for various hypothetical t-T paths (Fig. 8). Gradual cooling through the PbPRZ (~375-570°C) predicts an insufficient dispersion in U-Pb dates when compared with the actual measurements, and either isothermal holding or reheating are required to produce a sufficient dispersion. The large dispersion of dates that arises during reheating to temperatures within the bulk PbPRZ is a consequence of the combination of 100% retention of Pb in all grains prior to reheating, partial retention of Pb in large grains at the maximum temperature reached during reheating, and 100% loss of Pb in the smaller grains at the maximum temperature. The intra-grain U-Pb dates subsequently eliminate isothermal holding as a viable t-T solution (see section 5.4).

Utilizing lower crustal xenoliths collected from Archaean cratons, previous studies (Blackburn et al., 2011; Blackburn et al., 2012) have shown that U-Pb dates can be used to distinguish between slow cooling and reheating by comparing the topology of the U-Pb dates within concordia space (i.e. using both $^{207}Pb/^{235}U$ and $^{206}Pb/^{238}U$ dates). This has contributed significantly to understanding the long term stabilization of Archaean cratons (Blackburn et al., 2012). Unfortunately, this approach is limited to old U-Pb dates (e.g. >500 Ma) that span a large age range, permitting the user to resolve the topology of the Pb loss curves. This restriction is brought on by analytical constraints, yielding poor precision for relatively non-radiogenic isotopic compositions. In young samples (< 550 Ma), large age uncertainties such as those obtained in this study often result in concordant dates, despite the fact that they have demonstrably experienced lead loss, precluding the use of Pb loss curves in concordia space. However, we have demonstrated that U-Pb dates of single or multiple crystals, obtained using TIMS, can be used to differentiate between gradual cooling and reheating using only the ^{206}Pb

/^{238}U chronometer for dates as young as ~100 Ma. Schoene and Bowring (2007) demonstrated that the relationship between grain size and ^{238}U-^{206}Pb date for different mineral phases collected from the same hand specimen can also be used to distinguish between reheating and slow cooling in rocks that yield Archaean dates.

6.3 Combining TIMS dates, LA-ICP-MS dates and inversion modeling of t-T paths

Two main advantages arise when combining single crystal U-Pb dates obtained by TIMS and in-situ dates obtained by LA-ICP-MS. First, in this study, these different techniques were applied to different apatite crystals extracted from the same leucosome, and therefore both datasets are mainly independent of each other. Each dataset can then be used to construct statistically likely t-T solutions using a computed modeling approach. Concordance between the t-T solutions would imply that they are accurate, whereas distinguishable differences would raise doubts about their usefulness. Discrepancies in the t-T models may arise due to non-thermally activated, core-to-rim diffusion profiles, which could have formed by Pb loss during fluid interaction with the crystals. The in-situ dates may provide information about the cause of the discrepancy, by revealing, for example, a multi-domain structure created by the presence of lattice defects (e.g. Lee, 1995).

The second advantage is the ability of the combination of methods to distinguish between isothermal t-T paths, and reheating. In this example, inversion modeling of TIMS dates strongly favours reheating, although some isothermal paths are statistically permitted. However, isothermal holding is inconsistent with the in-situ U-Pb dates, leaving reheating as the only viable t-T solution.

7. Conclusions

1) The positive relationship between grain size and U-Pb dates obtained by TIMS, combined with consistent t-T paths derived from TIMS and MC-LA-ICP-MS data suggests that Pb was lost from apatites in the studied leucosome by thermally activated diffusion. Pb-loss by mechanisms that involve aqueous interaction are not required to account for the U-Pb dates.
2) Apatite grains with elevated Th/U ratios yield U-Pb dates that are younger than predicted from the relationship between grain size and date. The cause of the discrepancy is unknown, although it may be due to variations in intrinsic diffusion properties in apatites of varying composition. Alternatively, the young ages may be due to accelerated Pb-loss by processes that occur faster than thermally activated diffusion.
3) Sensible t-T paths have been obtained from Markov Chain Monte Carlo simulations of apatite U-Pb dates obtained by TIMS, using the HeFTy (Ketcham, 2005) software. The t-T paths span the Mesozoic, indicating that analytical constraints do not restrict the apatite U-Pb method to histories than have ages of ~500 Ma and older.
4) Inversion modeling of $^{206}Pb/^{238}U$ dates acquired by TIMS, and grain sizes is capable of distinguishing between reheating and gradual cooling paths. An additional comparison of predicted and measured in-situ $^{206}Pb/^{238}U$ dates permits isothermal holding to be distinguished from reheating paths. We conclude that a combination TIMS and LA-ICP-MS dates, with inversion modeling, is a powerful strategy to construct accurate t-T paths for time periods as young as 100 Ma.

References:

Baker, J., Peate, D., Waight, T. and Meyzen, C., 2004. Pb isotopic analysis of standards and samples using a 207Pb-204Pb double spike and thallium to correct for mass bias with a double-focusing MC-ICP-MS. Chemical Geology 211, 275-303.

Blackburn, T., Bowring, S., Schoene, B., Mahan, K. and Dudas, F., 2011. U-Pb thermochronology: creating a temporal record of lithosphere thermal evolution. Contributions to Mineralogy and Petrology 162, 479-500.

Blackburn, T.J. et al., 2012. An Exhumation History of Continents over Billion-Year Time Scales. Science 335, 73-76.

Boekhout, F. et al., 2012. Mesozoic arc magmatism along the southern Peruvian margin during Gondwana breakup and dispersal. Lithos 146-147, 48-64.

Bowring, J.F., McLean, N.M. and Bowring, S.A., 2011. Engineering cyber infrastructure for U-Pb geochronology: Tripoli and U-Pb_Redux. Geochem. Geophys. Geosyst., 12: Q0AA19.

Carlson, W.D., Donelick, R.A. and Ketcham, R.A., 1999. Variability of apatite fission-track annealing kinetics; I, Experimental results. American Mineralogist 84, 1213-1223.

Cassata, W.S., Renne, P.R. and Shuster, D.L., 2009. Argon diffusion in plagioclase and implications for thermochronometry: A case study from the Bushveld Complex, South Africa. Geochimica et Cosmochimica Acta 73, 6600-6612.

Chamberlain, K.R. and Bowring, S.A., 2001. Apatite-feldspar U-Pb thermochronometer: a reliable, mid-range (~ 450°C), diffusion-controlled system. Chemical Geology 172, 173-200.

Cherniak, D., 2010. Diffusion in Accessory Minerals: Zircon, Titanite, Apatite, Monazite and Xenotime. Reviews in Mineralogy and Geochemistry 72, 827-869.

Cherniak, D.J., Lanford, W.A. and Ryerson, F.J., 1991. Lead diffusion in apatite and zircon using ion implantation and Rutherford Backscattering techniques. Geochimica et Cosmochimica Acta 55, 1663-1673.

Cherniak, D.J., Watson, E.B., Grove, M. and Harrison, T.M., 2004. Pb diffusion in monazite: a combined RBS/SIMS study. Geochimica et Cosmochimica Acta 68, 829-840.

Chew, D.M., Petrus, J.A., and Kamber, B.S. (in press). U-Pb LA-ICPMS dating using accessory mineral standards with variable common Pb. Chemical Geology. doi 10.1016/j.chemgeo.2013.11.006

Chew, D.M., Sylvester, P.J. and Tubrett, M.N., 2011. U-Pb and Th-Pb dating of apatite by LA-ICPMS. Chemical Geology 280, 200-216.

Chu, M.-F., Wang, K.-L., Griffin, W. L., Chung, S.-L., O'Reilly, S. Y., Pearson, N. J., Iizuka, Y. 2009. Apatite Composition: Tracing Petrogenetic Processes in Transhimalayan Granitoids. Journal of Petrology 50, 1829-1855.

Cochrane, R., 2013. U-Pb thermochronology, geochronology and geochemistry of NW South America: Rift to drift transition, active margin dynamics and implications for the volume balance of continents. PhD thesis, University of Geneva, Switzerland, 118, 191 pp.

Dalrymple, B., G. and Lanphere, M., A., 1974. 40Ar/39Ar age spectra of some undisturbed terrestrial samples. Geochimica et Cosmochimica Acta 38, 715-738.

Dodson, M.H., 1973. Closure temperature in cooling geochronological and petrological systems. Contributions to Mineralogy and Petrology 40, 259-274.

Dodson, M.H., 1986. Closure profiles in cooling systems. Materials. Sci. Forum 7, 145-154.

Farley, K.A., Shuster, D.L. and Ketcham, R.A., 2011. U and Th zonation in apatite observed by laser ablation ICPMS, and implications for the (U-Th)/He system. Geochimica et Cosmochimica Acta 75, 4515-4530.

Gallagher, K., Brown, R. and Johnson, C., 1998. Fission track analysis and its applications to geological problems. Annual Review of Earth and Planetary Sciences 26, 519-572.

Gerstenberger, H. and Haase, G., 1997. A highly effective emitter substance for mass spectrometric Pb isotope ratio determinations. Chemical Geology 136, 309-312.

Harrison, T.M., Célérier, J., Aikman, A.B., Hermann, J. and Heizler, M.T., 2009. Diffusion of ^{40}Ar in muscovite. Geochimica et Cosmochimica Acta 73, 1039-1051.

Housh, T. and Bowring, S.A., 1991. Lead isotopic heterogeneities within alkali feldspars: Implications for the determination of initial lead isotopic compositions. Geochimica et Cosmochimica Acta 55, 2309-2316.

Jackson, S., 2008. LAMTRACE data reduction software for LA-ICP-MS. In: Sylvester, P.(Ed.), Laser ablation ICP-MS in the Earth Sciences: Current practices and outstanding issues. Short Course Series - Mineral. Assoc. Can. 40, 305-307

Ketcham, R.A., 2005. Forward and Inverse Modeling of Low-Temperature Thermochronometry Data. Reviews in Mineralogy and Geochemistry 58, 275-314.

Koppers, A.A.P., 2002. ArArCALC-software for 40Ar/39Ar age calculations. Computers & Geosciences 28, 605-619.

Krogh, T.E., 1973. A low-contamination method for hydrothermal decomposition of zircon and extraction of U and Pb for isotopic age determinations. Geochimica et Cosmochimica Acta 37, 485-494.

Lee, J.K.W., 1995. Multipath diffusion in geochronology. Contributions to Mineralogy and Petrology 120, 60-82.

Litherland, M., Aspden, J. and Jemielita, R.A., 1994. The metamorphic belts of Ecuador. British Geological Survey Overseas Memoir, 11(147).

Lovera, O.M., Grove, M., Mark Harrison, T. and Mahon, K.I., 1997. Systematic analysis of K-feldspar $^{40}Ar/^{39}Ar$ step heating results: I. Significance of activation energy determinations. Geochimica et Cosmochimica Acta 61, 3171-3192.

McDowell, F.W., McIntosh, W.C. and Farley, K.A., 2005. A precise 40Ar-39Ar reference age for the Durango apatite (U-Th)/He and fission-track dating standard. Chemical Geology 214, 249-263.

McLean, N.M., Bowring, J.F. and Bowring, S.A., 2011. An algorithm for U-Pb isotope dilution data reduction and uncertainty propagation. Geochemistry Geophysics Geosystems 12, Q0AA18.

Nutman, A.P., Friend, C.R.L., Horie, K. and Hikada, H., 2007. The Itsaq Gneiss Complex of southern West Greenland and its construction at convergent plate boundaries. Developments in Precambrian Geology, Oxford, pp. 15, 187-218.

Paton, C. et al., 2010. Improved laser ablation U-Pb zircon geochronology through robust downhole fractionation correction. Geochemistry Geophysics Geosystems 11, Q0AA06.

Petrus, J.A. and Kamber, B.S., 2012. VizualAge: A Novel Approach to Laser Ablation ICP-MS U-Pb Geochronology Data Reduction. Geostandards and Geoanalytical Research 36, 247-270.

Quidelleur, X. et al., 1997. Thermal evolution and slip history of the Renbu Zedong Thrust, southeastern Tibet. J. Geophys. Res. 102, 2659-2679.

Renne, P.R. et al., 1998. Intercalibration of standards, absolute ages and uncertainties in 40Ar/39Ar dating. Chemical Geology 145, 117-152.

Schoene, B. and Bowring, S.A., 2007. Determining accurate temperature-time paths from U-Pb thermochronology: An example from the Kaapvaal craton, southern Africa. Geochimica et Cosmochimica Acta 71, 165-185.

Sláma, J. et al., 2008. Plešovice zircon - A new natural reference material for U-Pb and Hf isotopic microanalysis. Chemical Geology 249, 1-35.

Spikings, R.A., Seward, D., Winkler, W., and Ruiz, G.M., 2000. Low-temperature thermochronology of the northern Cordillera Real, Ecuador: Tectonic insights from zircon and apatite fission track analysis. Tectonic 19, 649-668.

Spikings, R.A., Winkler, W., Seward, D. and Handler, R., 2001. Along-strike variations in the thermal and tectonic response of the continental Ecuadorian Andes to the collision with heterogeneous oceanic crust. Earth and Planetary Science Letters 186, 57-73.

Spikings, R.A., Crowhurst, P.V., Winkler, W. and Villagomez, D., 2010. Syn- and post-accretionary cooling history of the Ecuadorian Andes constrained by their in-situ and detrital thermochronometric record. Journal of South American Earth Sciences 30, 121-133.

Stacey, J.S. and Kramers, J.D., 1975. Approximation of terrestrial lead isotope evolution by a two-stage model. Earth and Planetary Science Letters 26, 207-221.

Steiger, R.H. and Jäger, E., 1977. Subcommission on geochronology: Convention on the use of decay constants in geo- and cosmochronology. Earth and Planetary Science Letters 36, 359-362.

Vallejo, C. et al., 2009. Mode and timing of terrane accretion in the forearc of the Andes in Ecuador. Geological Society of America Memoirs 204, 197-216.

Villa, I.M., 1998. Isotopic closure. Terra Nova 10, 42-47.

Villagomez, D. and Spikings, R., 2013. Thermochronology and tectonics of the Central and Western Cordilleras of Colombia: Early Cretaceous-Tertiary evolution of the Northern Andes. Lithos 160-161, 228-249.

Wartho, J.-A. et al., 1999. Direct measurement of Ar diffusion profiles in a gem-quality Madagascar K-feldspar using the ultra-violet laser ablation microprobe (UVLAMP). Earth and Planetary Science Letters 170, 141-153.

Watson, E.B. and Baxter, E.F., 2007. Diffusion in solid-Earth systems. Earth and Planetary Science Letters 253, 307-327.

Watson, E.B. and Cherniak, D.J., 2013. Simple equations for diffusion in response to heating. Chemical Geology 335, 93-104.

Weiss, B.P., Shuster, D.L. and Stewart, S.T., 2002 Temperatures on Mars from 40Ar/39Ar thermochronology of ALH84001. Earth and Planetary Science Letters 201. 465-472.

Wiedenbeck, M. et al., 1995. Three natural zircon standards for U-Th-Pb, Lu-Hf, trace element and REE analyses. Geostandards Newsletter 19, 1-23.

Williams, I.S., 1998. U-Th-Pb geochronology by ion microprobe. . Rev. Econ. Geol, 1-35.

Acknowledgments:

The authors acknowledge the assistance provided by Prof. Bernado Beate and Mr Luis López during field work in Ecuador, and Maria Ovtcharova and Michèle Senn for support with chromatographic separations and mass spectrometry. Careful and useful reviews were provided by D. Cherniak, T. Blackburn and an anonymous reviewer. An early version of the manuscript

benefited from suggestions from B. Watson and B. Schoene. Funds for the project were awarded to RS by the Swiss NSF (no. 200020_134443).

Appendix:

Analytical details: LA-ICP-MS zircon geochronology

U-Pb isotopic data was obtained from zircons extracted from leucosome RC42 using a CamScan MV2300 scanning electron microscope and suitable zircons were ablated using a NewWave UP-193 ArF excimer ablation system with a 25-35 um diameter beam size, 5 Hz repetition rate, 30-45 second signal and a beam intensity of 2.2-2.5 J/cm^2. Isotopic ratios of ablated zircons were measured using a Thermo Scientific Element XR. The GEMOC GJ-1 (CA-ID-TIMS $^{206}Pb/^{238}U$ age of 600.5 ± 0.4 Ma; Schaltegger et al., unpubl., in Boekhout et al. (2012) was used as a primary standard and ages were calculated using LAMTRACE (Jackson, 2008). External reference standards used to calibrate and monitor consistency in the measured Pb-U dates were either Harvard 91500 (1065.4 ± 0.3 Ma; Wiedenbeck et al., 1995) zircon, or Plešovice (337.13 ± 0.37 Ma; Sláma et al., 2008) zircon.

$^{40}Ar/^{39}Ar$ analysis

1 mg of muscovite was analysed (Table S2) by incremental step heating using a 55W CO_2-IR laser that was rastered over the sample to provide even-heating of the grains. The automated UHV stainless steel gas extraction line incorporates one SAES AP10 getter, one water-cooled, SAES GP50-ST101 getter and a cold-finger that is cooled 150 Kelvin. The gettered gas was analysed on a multi-collector mass spectrometer (Argus; Thermo Scientific) housed at the University of Geneva. The Argus is equipped with four high-gain (10^{12} ohms) faraday collectors for the analysis

of ^{39}Ar, ^{38}Ar, ^{37}Ar and ^{36}Ar, as well as a single faraday collector (10^{11} Ohms) for the analysis of ^{40}Ar. Samples were measured on the faraday collectors and time-zero regressions were fitted to data collected from twelve cycles. Peak heights and blanks were corrected for mass discrimination, isotopic decay of ^{39}Ar and ^{37}Ar and interfering nucleogenic Ca-, K- and Cl-derived isotopes. Error calculations include the errors on mass discrimination measurement, and the J value. ^{40}Ar, ^{39}Ar, ^{38}Ar, ^{37}Ar and ^{36}Ar blanks were calculated before every new sample and after every three heating steps. ^{40}Ar blanks were between 6.5E-16 and 1.0E-15 moles. Blank values for m/e 39 to 36 were all less than 6.5E-17 moles. The age plateau was determined using the criteria of (Dalrymple and Lanphere, 1974), and data reduction utilized ArArCalc (Koppers, 2002).

The isotopic composition of common Pb

Apatite crystals typically incorporate low quantities of uranium and significant amounts of lead during crystallization, resulting in low Pb^*/Pb_c in Phanerozoic samples (0.1 – 0.3 in this study). Therefore, an accurate knowledge of the initial Pb isotopic composition is required to obtain accurate and precise U-Pb dates. 10 mg of pure K-feldspar (previously separated using gravimetric and magnetic methods) was powdered in an agate mortar and leached for 12 hours with 1 ml of 6M HCl + 1 ml 14M HNO_3 at 120 °C. The leachate was discarded and the residue was rinsed twice with de-ionized H_2O before dissolution in 3 ml of concentrated HF + 1 ml 14M HNO_3 within a screw-sealed Teflon beaker at 160°C for 1 week. After complete dissolution of the K-feldspar powder, the solution was dried down and the residue was re-dissolved in 3 ml of 14M HNO_3 at 160°C for 3 days. The solution was finally dried down and dissolved in 1M HNO_3. Pb within the sample solution was purified using a macroporous AG-MP1-M resin before its isotopic composition was measured using a Neptune Plus MC-ICP-MS at the University of

Geneva (Switzerland). The analyses were done in static mode using a Tl solution (with a nominal $^{203}Tl/^{205}Tl$ value of 0.418922) for internal fractionation correction of Pb isotope ratios, while monitoring ^{202}Hg for the interference correction of ^{204}Hg on ^{204}Pb ($^{202}Hg/^{204}Hg = 4.35037$). The Pb isotope ratios were further corrected for external fractionation by 0.04% per amu with reference to the value of the SRM981 standard (Baker et al., 2004). The long-term (3 months) 1-sigma reproducibility of the SRM981 standard values are 0.006% for $^{206}Pb/^{204}Pb$, 0.005% for $^{207}Pb/^{204}Pb$ and 0.007% for $^{208}Pb/^{204}Pb$.

Figure captions

Fig. 1. Schematic illustration (not to scale) of the different mechanisms of displacement of Pb ions through a crystal (arrows depict movement direction). The crystal has ordered regions where the movement of ions can be described by Dodson's equations (in the case of cooling), resulting in the concept of closure temperature (Dodson, 1973), or by the equations of Watson and Cherniak (2013) for more complex cooling histories that include heating. Features such as crystal cleavage, lattice defects, exsolution and inclusion boundaries may provide pathways for aqueous fluid flow. The rate of loss of Pb in these "short-circuit" (Lee, 1995) pathways is dominantly controlled by aqueous fluid flow, and the mathematics of thermally activated diffusion must be modified to predict core-rim concentration profiles, especially when these pathways are inter-connected, provide access to the mineral surface and are perhaps enlarged by dissolution. The theoretical concentration profile (red line) for an ordered lattice was calculated for Pb in apatite with a diffusion radius of 100 microns, and equilibration at 450°C. The blue line schematically illustrates how the concentration of the daughter Pb ions may vary in a pathway that is fluid rich, where Pb loss occurs at a faster rate than by volume diffusion through the lattice.

Fig. 2. a: Locality of Triassic migmatite RC42 within the southern Eastern Cordillera of Ecuador, **b**: photograph showing the migmatite (Sabanilla Unit) in the southern Eastern Cordillera. **c**: U-Pb concordia plot for zircons extracted from a leucosome (RC42) of a migmatised, Permian sedimentary rock. All analyses performed by LA-ICP-MS.

Fig. 3. a: U-Pb concordia plot for apatite separated from a Triassic leucosome (zircon U-Pb 247±4.3 Ma). Black ellipses are U-Pb dates (TIMS) where the Pb_c composition was measured in co-genetic K-feldspar. These ellipses include propagated uncertainties of the initial Pb feldspar isotopic composition (1% on $^{206}Pb/^{204}Pb$, 0.5. % on $^{207}Pb/^{204}Pb$). We use these conservative uncertainty estimates to account for the inter- and intra-grain variability that is commonly observed in alkali feldspars (Table 1; Housh and Bowring, 1991). Asterisks indicate those size aliquots used to generate the t-T models. **b**: The positive correlation between $^{206}Pb/^{238}U$ date and diffusion length (defined as the orthogonal distance between the c-axis and the grain rim) supports the hypothesis that Pb loss occurred via thermally activated, volume diffusion. **c**: Two populations of apatite can be defined according to their Th/U ratios. Low Th/U (< 0.18) apatites are typical of magmatic apatite within S-type granites (Chu et al., 2009) and high Th/U (0.35 – 1.9) apatites are normally found within I-Type granites (Chu et al., 2009), suggesting that the high Th/U apatites in this study may be xenocrysts. Apatites with high Th/U apatites diverge from the trend of grain size versus $^{206}Pb/^{238}U$ date and yield relatively young $^{206}Pb/^{238}U$ dates. **d**: Photomicrographs (transmitted light) of selected apatites showing their subhedral-euhedral nature and grain size variation within leucosome RC42.

Fig. 4. LA-MC-ICP-MS $^{206}Pb/^{238}U$ date transects (A – A') for five apatite grains (coloured squares) with different grain size radii (130 – 50 um), and back-scatter electron images. Internal uncertainties on the dates are 2σ. Grains a and b exhibit significant uranium zonation (purple circles) and yield slightly concave core-rim date topologies, while grain c is less zoned and exhibits a convex date topology. Grain e has a constant core-rim uranium concentration and yields indistinguishable core-rim dates of ~67-70 Ma. The oldest dates obtained from grains b, c and d (which are taken as a proxy for the core and central axis of the grain) are offset from the center of the polished section, reflecting the effects of apatite tilting during the mounting process (f).

Fig. 5. $^{40}Ar/^{39}Ar$ age spectra for muscovites extracted from leucosome RC42. All uncertainties are ±2σ.

Fig. 6. a: A comparison of apatite grain radii (= diffusion lengths) and i) $^{206}Pb/^{238}U$ dates measured using TIMS (corrected for non-radiogenic Pb using co-genetic feldspar), and ii) predicted $^{206}Pb/^{238}U$ dates obtained from the best-fit t-T path (green path in Fig. 6b) obtained by inversion modeling. **b**: t-T paths (black) that satisfy the $^{206}Pb/^{238}U$ dates and grain sizes for the same 6 grain size aliquots (apatite) highlighted in Fig. 3a, simultaneously. The t-T solutions are forced to intercept the blue boxes (labeled 2, 3 and 4), and were derived by inverting the $^{206}Pb/^{238}U$ dates (assuming spherical geometry) using a controlled random search procedure using the software "HeFTy 1.7.0" (Ketcham, 2005). The red dashed line is added for effect and was not obtained from the modeling process. The red bar indicates the $^{40}Ar/^{39}Ar$ plateau muscovite age of the same leucosome (Fig. 5), and its ArPRZ (250μm diffusion length, dT/dt

20°C/Ma; Cherniak et al., 1991). PbPRZ: approximate bulk Pb Partial Retention Zone where the limits are Dodsonian closure temperatures (see text).

Fig. 7. A comparison of theoretical (coloured lines) and measured (transects a-e in Fig. 4, coloured squares; internal uncertainties only) Pb loss profiles from core to rim in apatite (values in boxes are grain radii in µm). Theoretical calculations assume i) constant U concentration from core to rim (solid lines), which was confirmed in three grains (see Fig. 4), or ii) varying U concentration from core to rim (dashed lines enclosing a grey envelope), which was found in grains a and b (Fig. 4). **a**: Pb loss profile derived from the best fit t-T solution (Fig. 6b) reveals a significant spread in $^{206}Pb/^{238}U$ dates of > 60% between the cores and rims of the largest grains, which is resolvable and is confirmed by LA-MC-ICP-MS dating. No distinguishable variation in $^{206}Pb/^{238}U$ dates is found between the cores and rims of the smallest apatites. **b**: theoretical $^{206}Pb/^{238}U$ dates derived from isothermal holding at temperatures in the mid-point of the PbPRZ, followed by the lowest cooling rate permitted out of the bulk PbPRZ as constrained by the muscovite $^{40}Ar/^{39}Ar$ date, predict more Pb loss at the rims of the smaller grains than what is measured, and **c:** theoretical $^{206}Pb/^{238}U$ dates derived from isothermal holding at temperatures in the mid-point of the PbPRZ, followed by the highest cooling rate permitted out of the bulk PbPRZ as constrained by the muscovite $^{40}Ar/^{39}Ar$ date, also predict more Pb loss at the rims of the smaller grains than what is measured**, d**: slow cooling at a constant rate (1.25°C/My) does not match the profiles found from LA-MC-ICP-MS dating. This data set demonstrates the importance of using apatite grains that have radii of 60 µm or smaller, when attempting to resolve between slow cooling and reheating to temperatures within the mid-point of the PbPRZ.

Fig. 8. a: Synthetic t-T paths (labeled 1 to 7) that have been used to generate model $^{206}Pb/^{238}U$ dates by forward modeling (see b) for apatite grains which have the same range in grain sizes (diffusion lengths) as those used in the current study. **b**: A comparison of forward modeled and measured $^{206}Pb/^{238}U$ (yellow symbol-uncertainty; see Fig. 3a) dates. The gray region shows data obtained from the best-fit paths shown in Fig. 6b. Cooling paths with varying cooling rates into and through the PbPRZ from temperatures higher than the PbPRZ (labeled 1 to 5 in a) do not produce a sufficient dispersion in dates, relative to the measured dates. Reheating and isothermal solutions are required to generate a close match between the modeled and measured dates. The large dispersion found in the measured dates is a consequence of i) radiogenic Pb in-growth in all grains while at temperatures colder than the PbPRZ, for a prolonged time period of ~100 million years, ii) partial resetting of the larger grains during reheating, and iii) complete resetting of the smaller grains during reheating.

Table 1. U-Pb isotopic data of apatites extracted from a Triassic migmatite (RC42). Data obtained using isotope dilution thermal ionization mass spectrometry (ID-TIMS).

Table 2. Laser ablation multi-collector inductively coupled mass spectrometer (LA-MC-ICP-MS) data acquired from apatites (crystals A-E) extracted from Triassic migmatite RC42.

Supplementary Materials:

Fig. S1. The temperature boundaries of the Pb Partial Retention Zone (PbPRZ) in apatite for spherical (dark grey band) and infinite cylinder geometries. Calculations were made using the

physical parameters (absolute diffusivity and activation energy) of Cherniak et al. (1991), a cooling rate of 20°C/Ma, and an effective diffusion radii of 30-150 μm. The variation in the temperature bounds of the PbPRZ is insignificant when using spherical or infinite cylinder geometry

Fig. S2. The relationship between the temperature bounds of the PbPRZ and grain sizes of the apatites utilized in this study. The PbPRZ is calculated using the physical parameters (absolute diffusivity and activation energy) of Cherniak et al. (1991), a cooling rate of 20°C/Ma, effective diffusion radii for the six modeled apatites in this study, and a spherical geometry. Labels are grain radii in microns.

Supplementary Table 1. Laser ablation inductively coupled mass spectrometer (LA-ICP-MS) U-Pb dates acquired from zircons extracted from Triassic migmatite RC42.

Supplementary Table 2. Argon isotope data obtained from muscovite of leucosome RC42.

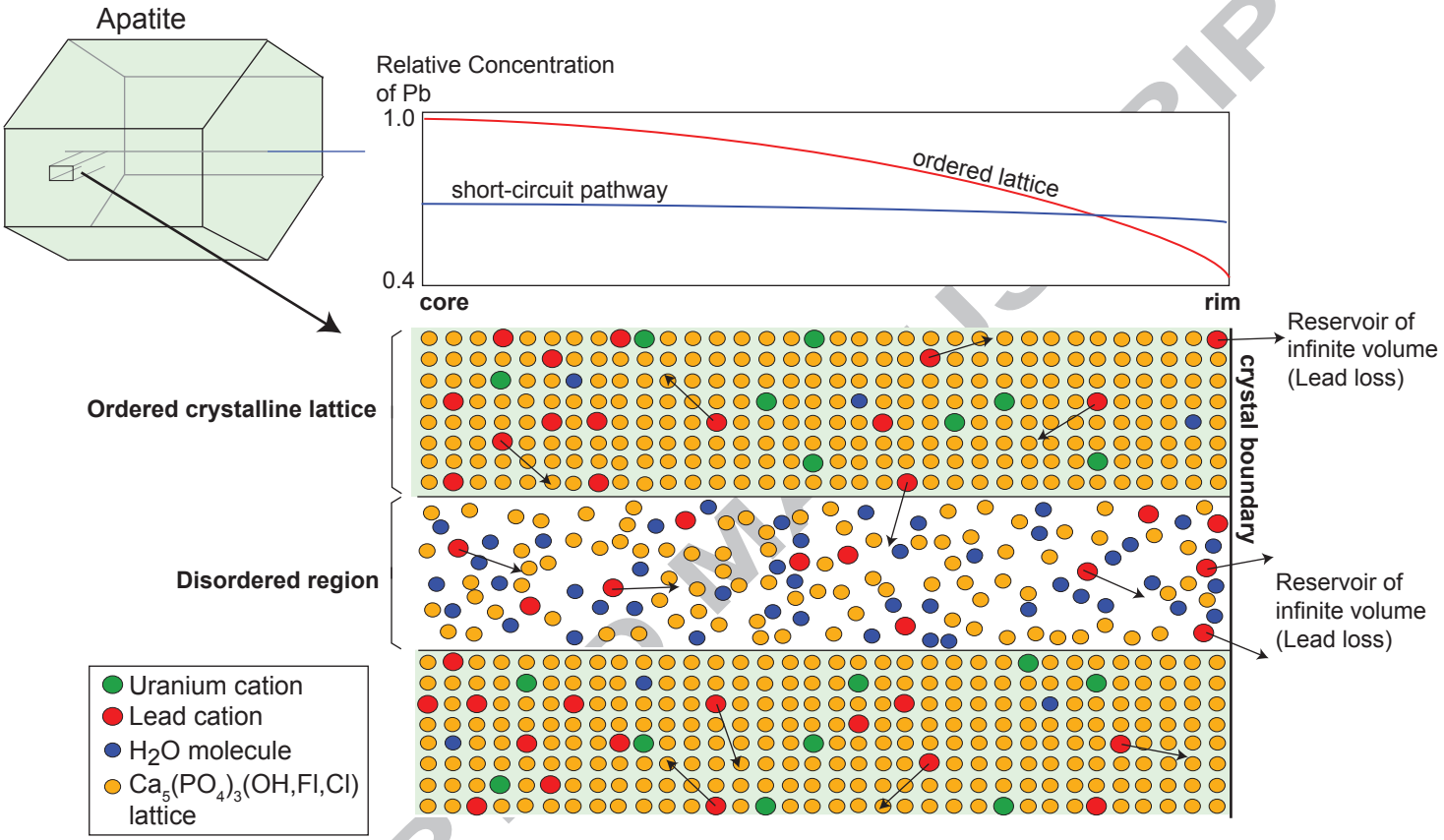

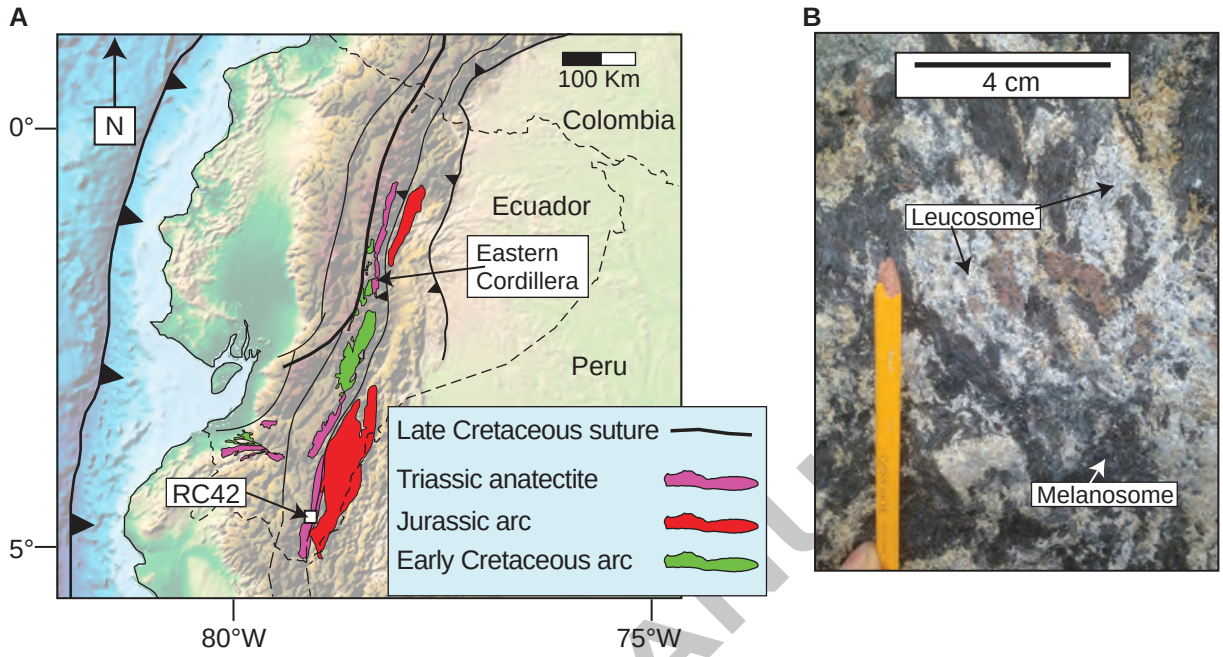

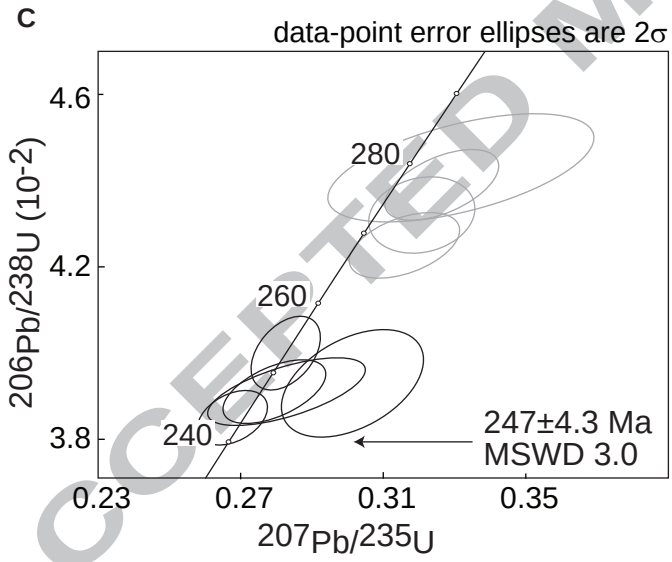

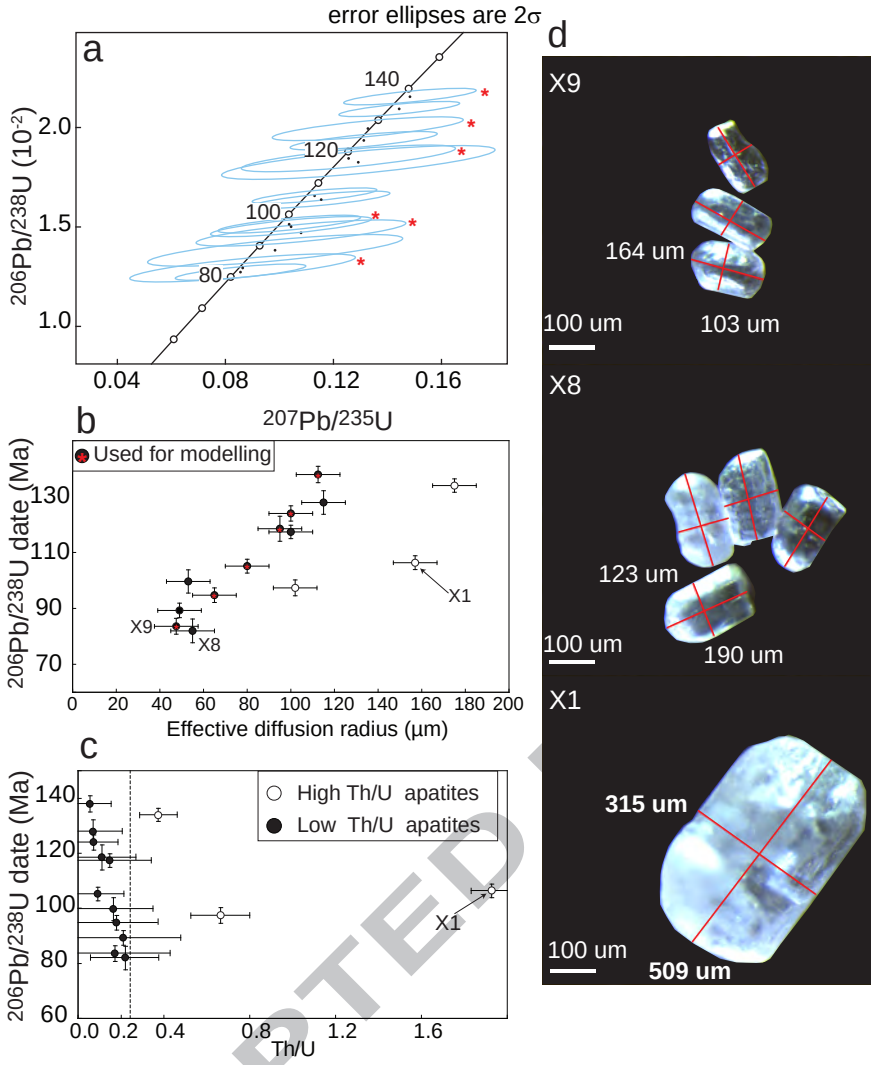

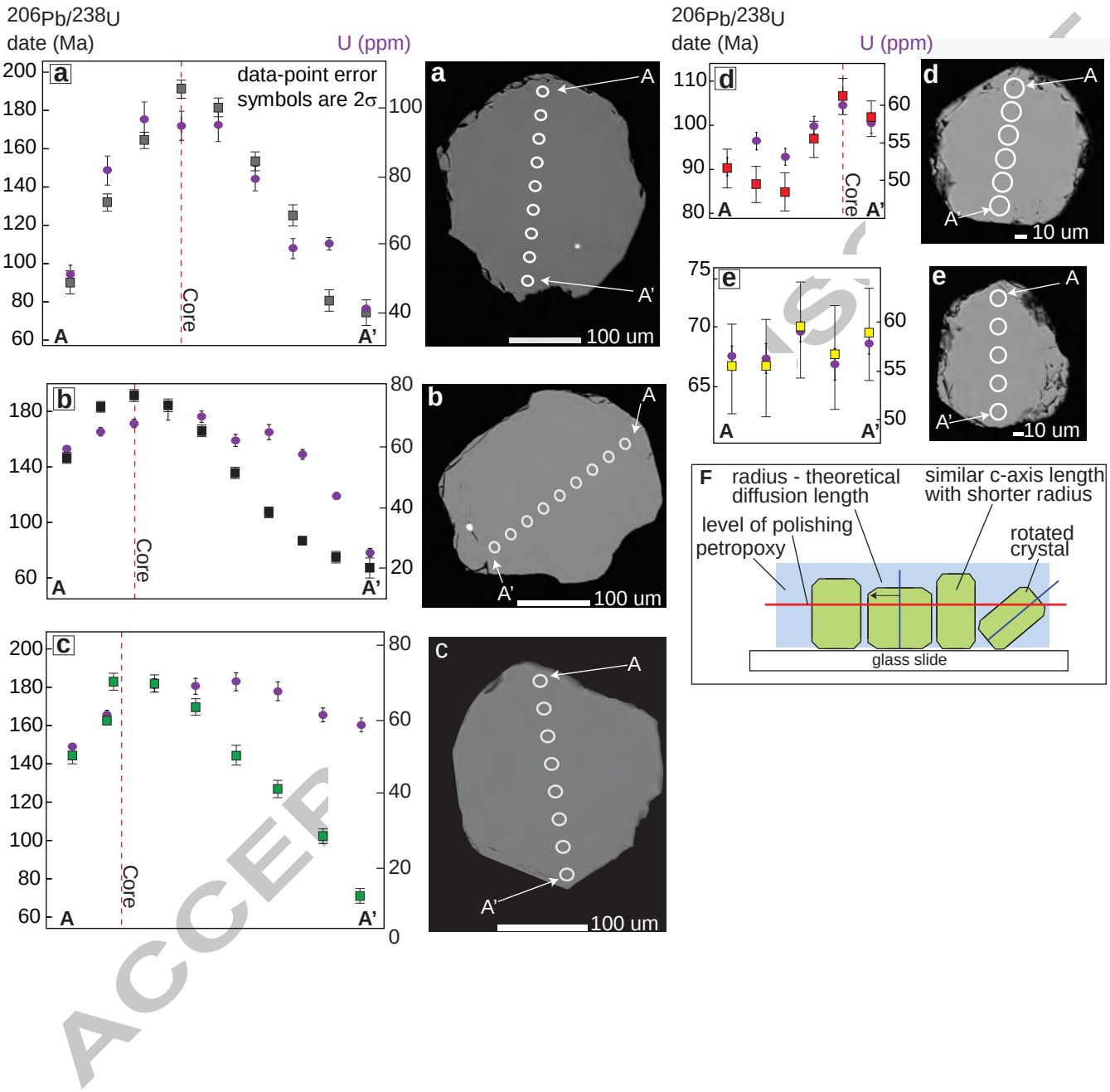

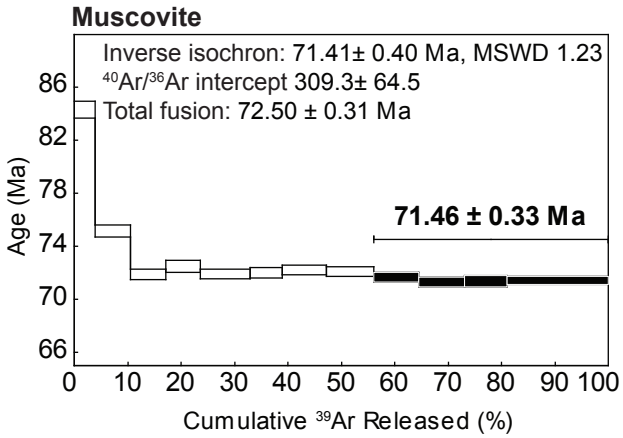

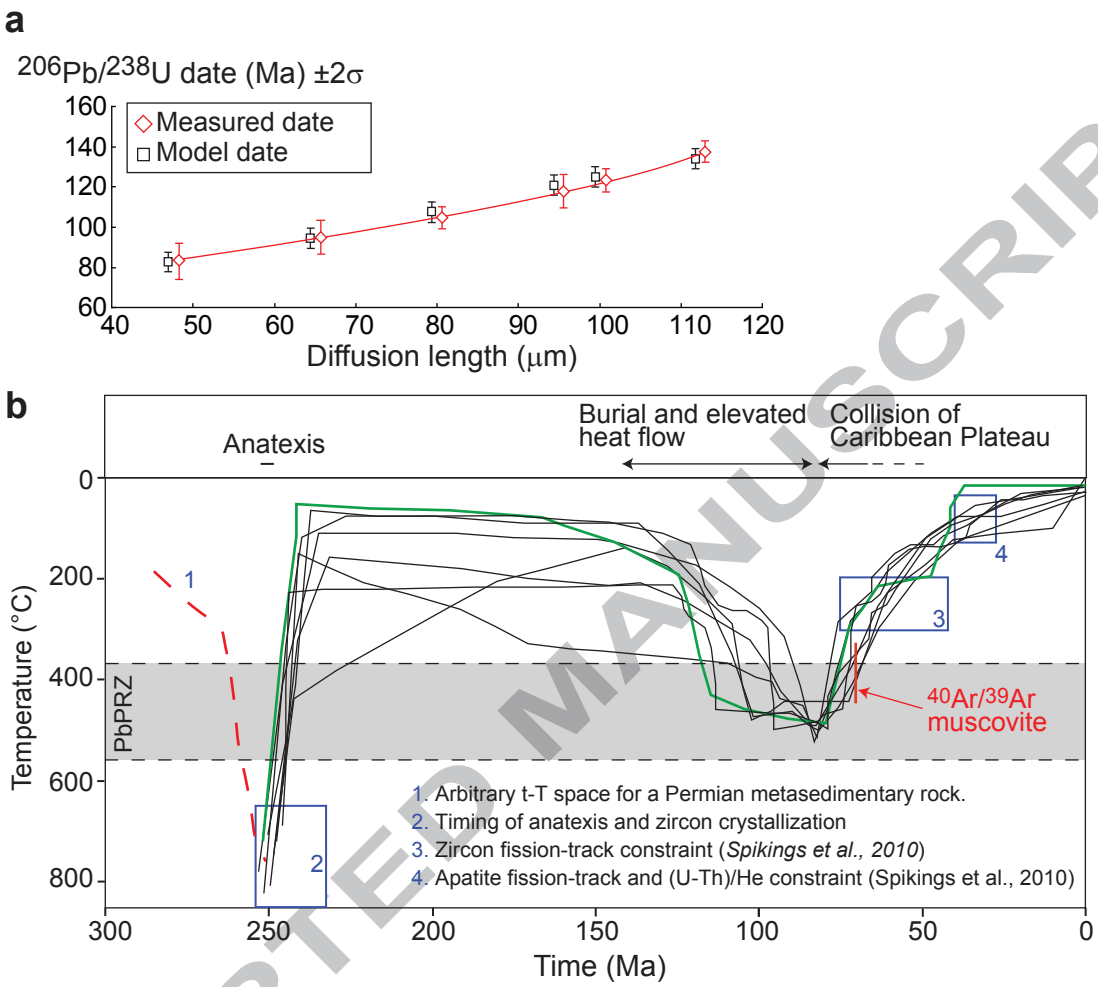

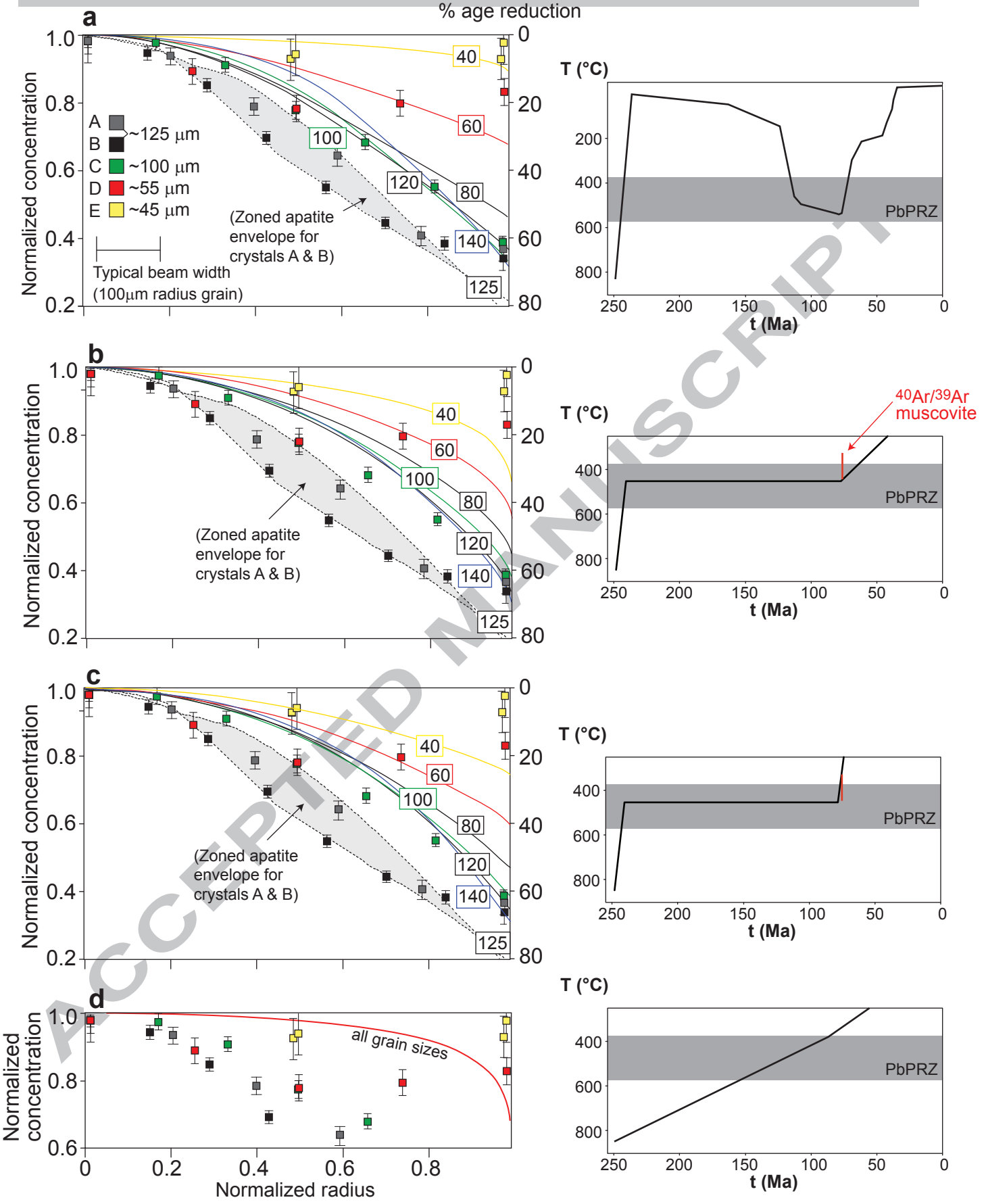

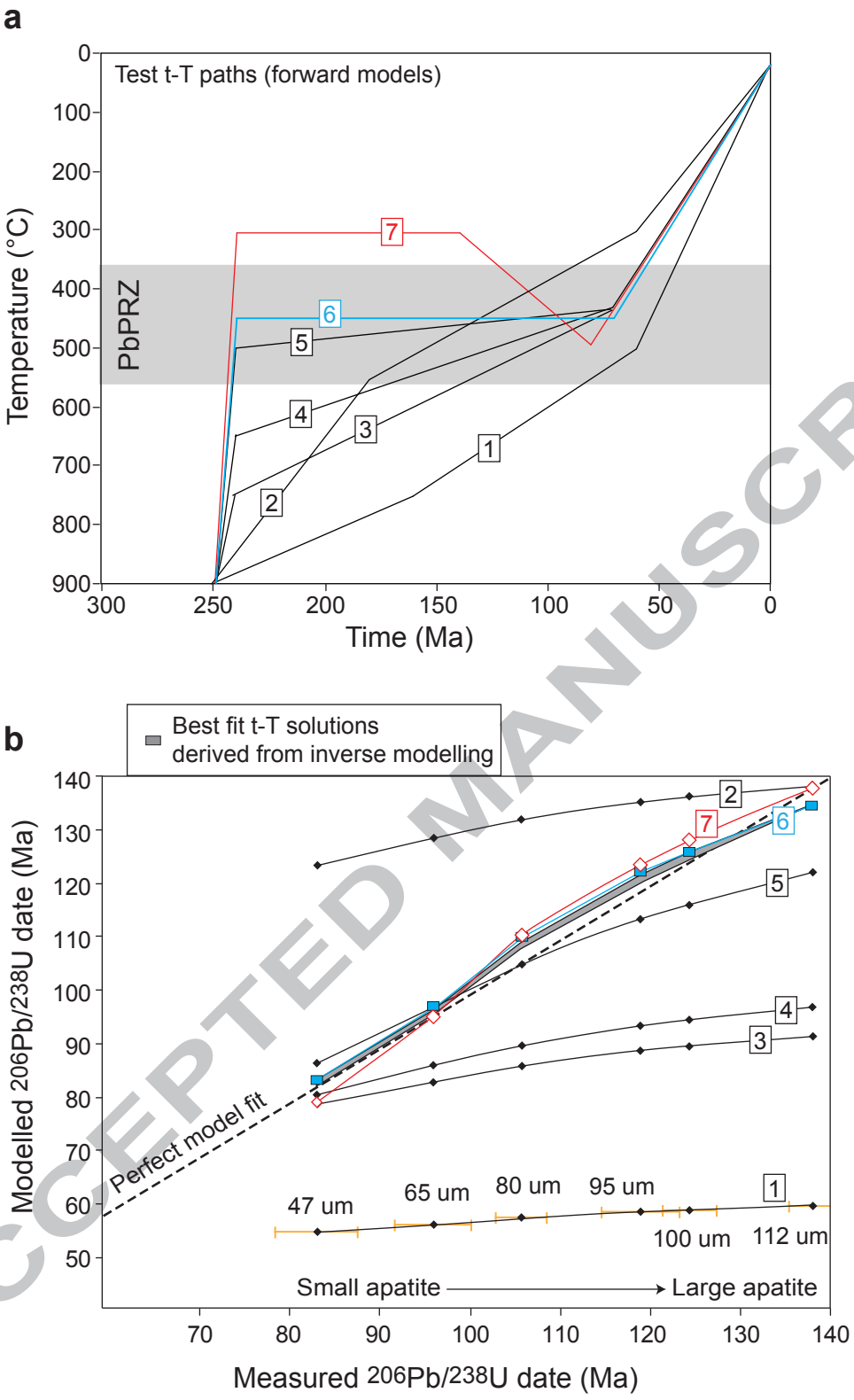

Table 1. U-Pb isotopic data (feldspar Pb_c corr)

RC42								Isotopic ratios								Dates (Ma)	
Apatite	# grains	Grain radius [μm] ±10μm [a]	Th/U [b]	±2σ	Pb* (pg) [c]	Pbc (pg) [d]	Pb*/Pbc [e]	$^{206}Pb/^{204}Pb$ [f]	$^{206}Pb/^{238}U$ [g]	±2σ %	$^{207}Pb/^{235}U$ [g]	±2σ %	$^{207}Pb/^{206}Pb$ [g]	±2σ %	Corr. coef.	$^{206}Pb/^{238}U$ [h]	±2σ absi
X1	1	158	1.90	0.09	64.6	181.7	0.36	34.3	0.0166	2.37	0.1130	20.4	0.04945	18.7	0.750	105.9	2.5
X2	2	80	0.06	0.13	14.6	71.7	0.20	32.6	0.0164	2.63	0.1155	22.0	0.05115	20.1	0.750	104.7	2.7
X3	3	100	0.04	0.12	35.0	155.8	0.22	34.1	0.0193	2.39	0.1312	20.8	0.04920	19.0	0.750	123.5	2.9
X4	1	112	0.03	0.09	16.8	61.2	0.28	37.6	0.0216	1.93	0.1483	16.5	0.04991	15.1	0.751	137.5	2.6
X5	3	65	0.13	0.22	9.8	79.5	0.12	26.8	0.0147	4.47	0.1080	36.0	0.05329	32.7	0.749	94.0	4.2
X6	≤3	53	0.11	0.21	2.8	23.1	0.12	26.8	0.0155	4.36	0.1099	36.5	0.05153	33.4	0.748	98.9	4.3
X7	≤3	102	0.63	0.14	34.6	161.8	0.21	31.1	0.0151	2.96	0.1037	25.5	0.04965	23.3	0.749	96.9	2.8
X8	≤4	55	0.18	0.16	20.8	119.9	0.17	30.1	0.0127	3.22	0.0856	28.2	0.04878	25.9	0.749	81.5	2.6
X9	≤3	47	0.11	0.27	5.2	52.0	0.10	25.3	0.0129	5.45	0.0864	48.4	0.04840	44.4	0.749	82.9	4.5
X10	1	49	0.14	0.29	1.8	19.4	0.09	24.7	0.0138	5.77	0.0984	48.0	0.05163	43.8	0.748	88.5	5.1
X11	≤2	95	0.07	0.18	4.1	28.1	0.14	28.5	0.0184	3.64	0.1255	31.6	0.04936	29.0	0.749	117.8	4.2
X12	1	175	0.35	0.09	68.0	209.6	0.32	39.1	0.0209	1.82	0.1444	15.5	0.05003	14.2	0.750	133.5	2.4
X32	1	115	0.03	0.15	6.6	37.7	0.18	30.8	0.0199	2.99	0.1327	26.6	0.04827	24.5	0.749	127.2	3.8
X52	1	100	0.09	0.23	2.0	18.1	0.11	26.2	0.0182	4.66	0.1292	39.2	0.05137	35.8	0.747	116.5	5.4

Feldspar Pb isotopic data

weight (μg)	$^{206}Pb/^{204}Pb$	±2σ abs_i	$^{207}Pb/^{204}Pb$	±2σ abs_i	$^{208}Pb/^{204}Pb$	±2σ abs_i
10	18.581	0.1858	15.643	0.0782	38.536	0.5780

a Apatite grain radius measured normal to c-axis and considered to be the effective diffusion length.

b Th contents calculated from radiogenic ^{208}Pb and the $^{207}Pb/^{206}Pb$ date of the sample, assuming concordance between the U-Th and Pb systems.

c Total mass of radiogenic Pb.

d Total mass of common Pb.

e Ratio of radiogenic Pb (including ^{208}Pb) to common Pb.

f Measured ratio corrected for fractionation and spike contribution only.

g Measured ratios corrected for fractionation, tracer, blank and initial common Pb.

h Isotopic dates calculated using the decay constants λ238 = 1.55125E-10/a and λ235 = 9.8485E-10/a (Jaffey et al. 1971).

i All U-Pb isotopic ratios, and dates are corrected for initial common Pb using measured alkali feldpar Pb isotopic composition (reported at bottom of the table) with uncertainties assigned to $^{206}Pb/^{204}Pb$ (1.0%), $^{207}Pb/^{204}Pb$ (0.5%) and $^{208}Pb/^{204}Pb$ (1.5%) to account for natural feldspar variations (Housh and Bowring, 1991).

Table 2. U-Pb LA-MC-ICP-MS isotopic data from apatite (leucosome RC42)

RC42		Isotopic ratios							Isotopic dates (Ma)		(ppm)	
Apatite$_a$	Transect	$^{207}Pb/^{235}U$	$\pm2\sigma_b$	$^{206}Pb/^{238}U$	$\pm2\sigma_b$	Rho	$^{207}Pb/^{206}Pb$	$\pm2\sigma_b$	$^{206}Pb/^{238}U_c$	$\pm2\sigma_b$	U	$\pm2\sigma_b$
A	A	4.010	0.032	0.048	0.0003	0.863	0.610	0.003	90.1	5.6	56	2.6
		3.046	0.035	0.046	0.0004	0.965	0.485	0.002	132.0	4.3	86	4
		2.754	0.042	0.048	0.0006	0.975	0.417	0.002	164.6	4.2	100	4.8
		3.076	0.041	0.055	0.0006	0.984	0.409	0.002	191.3	4.5	98	4.2
		3.050	0.051	0.053	0.0007	0.981	0.417	0.002	181.7	4.7	99	4.5
		3.016	0.067	0.049	0.0008	0.968	0.451	0.003	153.5	4.9	83	3.3
		3.781	0.034	0.051	0.0004	0.929	0.538	0.003	125.3	5.3	59	2.7
		3.029	0.081	0.038	0.0007	0.943	0.575	0.011	80.8	5.4	64	1.6
	A'	4.497	0.093	0.050	0.0007	0.965	0.657	0.004	74.5	6.5	43	1
B	A	2.362	0.038	0.043	0.0005	0.896	0.409	0.003	148.1	3.6	59	1
		2.476	0.025	0.049	0.0004	0.860	0.370	0.002	184.7	3.5	65	1.4
		2.445	0.037	0.050	0.0007	0.946	0.357	0.002	192.9	4.0	67	1.4
		2.388	0.035	0.048	0.0007	0.954	0.360	0.002	185.8	4.0	70	1.5
		2.281	0.033	0.045	0.0006	0.939	0.374	0.002	167.4	3.8	70	1.9
		2.364	0.027	0.041	0.0006	0.918	0.423	0.002	137.3	3.7	62	2
		2.229	0.042	0.035	0.0006	0.951	0.458	0.004	108.9	3.6	64	2.5
		2.184	0.040	0.032	0.0004	0.955	0.498	0.004	88.6	3.3	57	1.6
		2.650	0.043	0.034	0.0005	0.922	0.563	0.003	76.8	3.8	44	1.2
	A'	4.597	0.078	0.050	0.0006	0.878	0.671	0.007	69.0	6.9	25	1.3
C	A	2.625	0.048	0.044	0.0006	0.945	0.432	0.002	145.4	4.1	49	0.92
		2.502	0.043	0.049	0.0007	0.952	0.373	0.002	183.9	4.2	58	1.2
		2.505	0.045	0.049	0.0008	0.977	0.373	0.002	183.0	4.3	66	1.5
		2.535	0.039	0.047	0.0007	0.967	0.390	0.002	170.8	4.1	65	2
		2.355	0.071	0.042	0.0011	0.984	0.408	0.003	145.6	5.0	66	2.2
		2.439	0.065	0.040	0.0008	0.982	0.444	0.003	127.9	4.3	64	2.3
		2.342	0.045	0.035	0.0006	0.954	0.480	0.003	103.3	3.6	57	1.7
	A'	2.422	0.049	0.031	0.0006	0.954	0.557	0.004	72.0	3.6	55	1.7
D	A	3.029	0.047	0.039	0.0005	0.927	0.557	0.003	90.0	4.3	52	1.2
		2.847	0.041	0.037	0.0005	0.923	0.554	0.003	86.4	4.0	55	1.2
		2.961	0.051	0.038	0.0006	0.934	0.564	0.003	84.7	4.2	53	1.1
		2.801	0.042	0.038	0.0005	0.931	0.529	0.003	96.7	4.0	57	1.2

		2.713	0.048	0.039	0.0006	0.948	0.502	0.003	106.4	4.0	60	1.2
	A'	2.765	0.041	0.039	0.0005	0.917	0.516	0.003	101.3	3.9	58	1.3
	A	2.532	0.055	0.032	0.0006	0.962	0.580	0.003	66.5	3.7	56	0.98
		2.715	0.063	0.033	0.0007	0.969	0.593	0.004	66.6	4.0	56	1.5
E		2.547	0.077	0.032	0.0008	0.976	0.572	0.004	69.7	4.0	59	0.99
		2.842	0.081	0.034	0.0008	0.980	0.596	0.005	67.4	4.3	56	1.6
	A'	2.601	0.054	0.033	0.0006	0.959	0.578	0.003	69.4	3.8	58	1.1

Table 2b. LA-MC-ICP-MS standard apatite data

	Isotopic ratios							Isotopic dates (Ma)			(ppm)	
Apatite	$^{207}Pb/^{235}U$	$\pm2\sigma_b$	$^{206}Pb/^{238}U$	$\pm2\sigma_b$	Rho	$^{207}Pb/^{206}Pb$	$\pm2\sigma_b$	$^{206}Pb/^{238}U_c$	$\pm2\sigma_b$	U	$\pm2\sigma_b$
Durango	0.144	0.008	0.00591	0.000088	0.165	0.1764	0.0097	31.76	0.681	18.5	0.87
	0.155	0.008	0.00602	0.000094	0.103	0.1850	0.0094	31.96	0.699	17.7	0.84
	0.159	0.007	0.00595	0.000090	0.184	0.1914	0.0089	31.28	0.663	16.9	0.78
	0.148	0.008	0.00596	0.000089	0.123	0.1788	0.0093	31.91	0.674	17.3	0.79
	0.140	0.008	0.00574	0.000096	0.204	0.1767	0.0094	30.82	0.693	19.4	0.79
	0.151	0.007	0.00575	0.000087	0.122	0.1899	0.0083	30.27	0.623	20.0	0.95
	0.139	0.006	0.00580	0.000093	0.106	0.1710	0.0077	31.41	0.637	20.8	0.99
	0.147	0.006	0.00576	0.000079	0.185	0.1828	0.0077	30.67	0.576	20.6	0.96
	0.157	0.006	0.00576	0.000078	0.181	0.1927	0.0078	30.18	0.574	20.4	0.96
	0.151	0.006	0.00583	0.000095	0.132	0.1867	0.0083	30.85	0.659	20.8	0.95
	0.150	0.007	0.00575	0.000110	0.208	0.1845	0.0085	30.53	0.724	21.8	0.95
	0.155	0.006	0.00592	0.000092	0.095	0.1875	0.0074	31.28	0.625	20.6	0.94
								31.08	**0.652**		
Emerald Lake	2.842	0.024	0.03761	0.000230	0.430	0.5516	0.0045	87.95	4.103	19.5	0.7
	2.777	0.026	0.03682	0.000300	0.506	0.5525	0.0049	85.84	4.090	20.1	0.68
	2.846	0.019	0.03797	0.000180	0.127	0.5448	0.0043	90.86	4.058	19.5	0.67
	2.863	0.018	0.03811	0.000170	0.073	0.5453	0.0042	91.04	4.064	19.7	0.7
	2.721	0.020	0.03675	0.000190	0.259	0.5362	0.0042	90.49	3.864	21.1	0.64
	2.751	0.020	0.03674	0.000200	0.355	0.5421	0.0041	88.73	3.898	22.0	0.88
	2.930	0.023	0.03856	0.000210	0.263	0.5491	0.0045	90.93	4.180	19.7	0.62
	2.939	0.021	0.03882	0.000190	0.090	0.5459	0.0045	92.54	4.178	20.1	0.69
	2.921	0.021	0.03878	0.000180	0.231	0.5421	0.0042	93.63	4.113	20.3	0.72
	2.969	0.021	0.03931	0.000190	0.232	0.5419	0.0041	94.97	4.159	19.9	0.65
	3.025	0.027	0.03994	0.000250	0.441	0.5451	0.0043	95.45	4.287	19.2	0.55
	2.948	0.020	0.03933	0.000170	0.118	0.5383	0.0047	96.15	4.192	20.2	0.69

	91.55	**4.099**

a Apatite crystals A-E analysed from rim-core-rim (see Figure 4).
b Internal errors.
c ^{207}Pb corrected dates employing a common Pb composition of $^{207}Pb/^{206}Pb$ = 0.84188 (measured from co-genetic feldspar). A conservative 2σ uncertainty of 0.02 (abs) is propagated through the ^{207}Pb correction. Changing the common lead composition by ± 0.02 systematically shifts the ages the ages by about ± 4 Ma.